NANO LETTERS

2008
Vol. 8, No. 2
544−550

Peeling Force Spectroscopy: Exposing the Adhesive Nanomechanics of One-Dimensional Nanostructures

M. C. Strus,[†] L. Zalamea,[‡] A. Raman,*[,†] R. B. Pipes,[§] C. V. Nguyen,[||] and E. A. Stach[‡]

School of Mechanical Engineering and Birck Nanotechnology Center, School of Material Science and Engineering, Schools of Aeronautics and Astronautics, Chemical Engineering, and Material Science and Engineering, Purdue University, West Lafayette, Indiana, and ELORET Corporation, NASA Ames Research Center, Moffett Field, California

Received October 30, 2007; Revised Manuscript Received December 18, 2007

ABSTRACT

The physics of adhesion and stiction of one-dimensional nanostructures such as nanotubes, nanowires, and biopolymers on different material substrates is of great interest for the study of biological adhesion and the development of nanoelectronics and nanocomposites. Here, we combine theoretical models and a new mode in the atomic force microscope to investigate quantitatively the physics of nanomechanical peeling of carbon nanotubes and nanocoils on different substrates. We demonstrate that when an initially straight nanotube is peeled from a surface, small perturbations can trigger sudden transitions between different geometric configurations of the nanotube with vastly different interfacial energies. This opens up the possibility of quantitative comparison and control of adhesion between nanotubes or nanowires on different substrates.

The mechanical peel test is a routine experiment utilized by industry to measure macroscopic adhesive strength[1] and thin-film microscopic bonding.[2] Until now, no such test exists at the nanoscale, where it would be of great interest to the study of setae adhesion in geckos,[3] protein filament adhesion in mussels,[4] scaffolding construction for cell growth,[5] DNA and biomolecular templates,[6] nanofiber dispersion,[7] carbon nanotube-tipped AFM probes,[8] nanoswitches and nanotweezers,[9,10] nanoscale sensors,[11] and nanotube-matrix interactions in nanocomposites.[12−15]

At the nanoscale, the peeling of long slender molecules and nanostructures from substrates involves a strong coupling between elasticity, friction, and adhesive forces. Thus, the nanoscale peel test requires the ability to manipulate and displace slender nanostructures with nanoscale precision while monitoring extremely small forces. The atomic force microscope (AFM) is uniquely suited for such a test and is commonly used for measuring the mechanical properties of cells and proteins by pushing[16,17] or pulling[18,19] on surfaces or molecules.

In this work, we use a theoretical model and adapt the AFM to investigate the adhesive nanomechanics of one-dimensional nanostructures such as straight carbon nanotubes (CNTs) and carbon nanocoils as they are peeled from different substrates. Unlike at the macroscale,[20] we show that an initially straight CNT peeling from a substrate undergoes multiple sudden transitions between different geometric configurations characterized by sequentially decreasing interfacial energies. The coexistence of and transitions between such configurations naturally suggest intriguing possibilities for controlling stiction in artificial gecko setae,[21] nanoelectromechanical-based switches for flash memories,[22] and for the effective dispersion of CNTs and nanofibers in the manufacture of nanocomposites.[23] These peeling force spectrograms are very sensitive to the substrate material and are capable of resolving differences in interfacial energies at attoJoule levels. This opens up the possibility of highly sensitive characterization and screening of different nanotube/nanowire/nanofiber and substrate combinations for desired adhesion properties.

To better understand the fundamental physics underpinning the process, a computational model was developed to predict the nanomechanical peeling of CNTs. The CNT was modeled as an inextensible elastica[24] interacting via the "universal graphitic potential" with a graphite substrate.[25] For the universal graphitic potential to be valid, the substrate and

* Corresponding author.
[†] School of Mechanical Engineering and Birck Nanotechnology Center, Purdue University.
[‡] School of Material Science and Engineering, Purdue University.
[§] Schools of Aeronautics and Astronautics, Chemical Engineering, and Material Science and Engineering, Purdue University.
[||] ELORET Corporation, NASA Ames Research Center.

10.1021/nl0728118 CCC: $40.75
Published on Web 01/12/2008

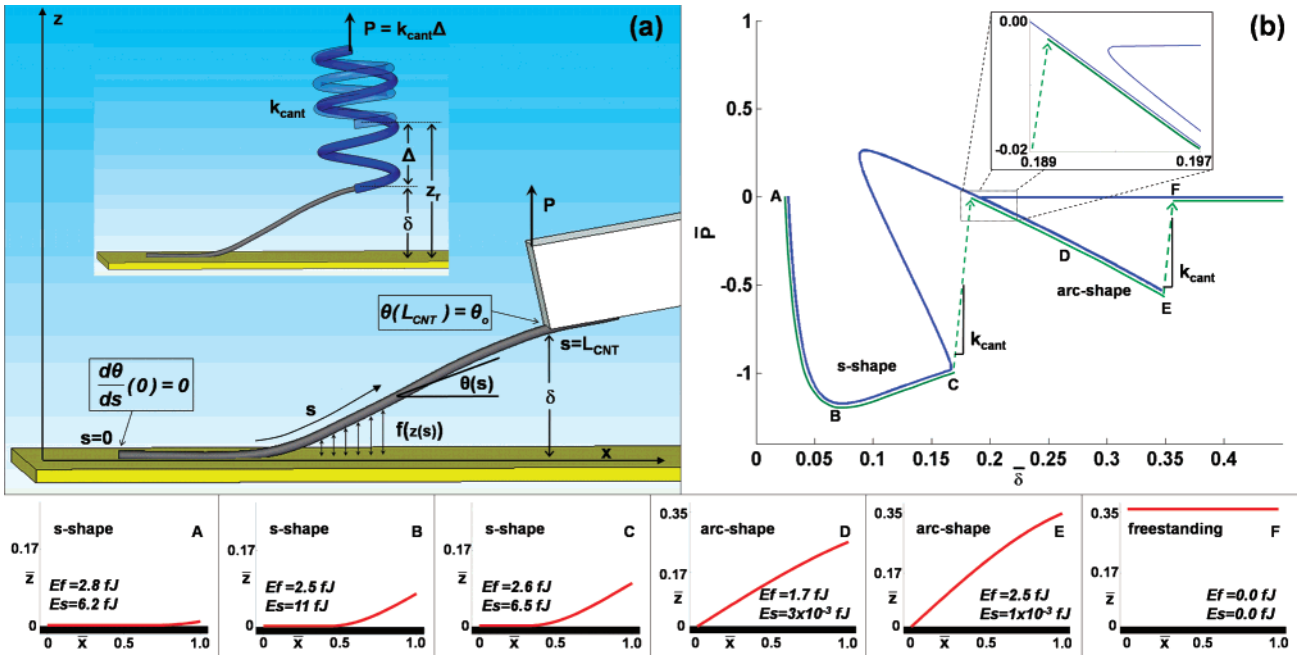

Figure 1. (a) A computational model using the inextensible elastica[24] for the nanotube and Girifalco's[25] universal graphitic potential is developed to predict the peeling of carbon nanotubes on HOPG. Specifically, the interaction forces are assumed to act only between the outermost nanotube shell and the surface, while all the shells contribute to the bending stiffness of the nanotube. In (b) the nondimensional applied peeling force, $\bar{P}$, is plotted against the nondimensional separation, $\bar{\delta}$, of the force-applied peeling point from the substrate using the following parameters that are fairly representative of the multiwalled CNT probes studied in experiments: $\alpha = 0.22$, $L_{CNT} = 1.5\ \mu$m, $E_{CNT} = 100$ MPa, $d_o = 10$ nm, $d_i = 41$ nm, $\theta_o = 11°$, $\Phi_o = 14$ nN. The area moment of the CNT was calculated using $I_{CNT} = \pi/64(d_o^4 - d_i^4)$. As indicated by the dotted line, the results clearly predict discontinuous transitions between s-shape, arc-shape, and freestanding CNT configurations upon retraction, as shown by the CNT configurations A−F. The applied force does work to the system to overcome the instantaneous energy stored elastically (E_f) and the interfacial energy (E_s).

CNT must have negligible surface roughness, a reasonable assumption for a freshly cleaved high-order pyrolitic graphite surface and CNT's with small diameter. Surfaces or fibers with larger roughness would require models that account for the short range interaction at and between asperities.[26] Inextensible elastica rod models have been useful in approximating the deformation of nanofibers, biopolymers, and nanotubes.[27−29] Because of the exceptionally high axial elastic modulus of CNTs,[30] axial deformation is negligible compared to flexure. Thus, the applied forces required to peel a CNT must overcome the elastica-substrate interaction potential while accounting for bending.

Figure 1a shows the CNT modeled as an elastica with arc length parameter s varying from $s = 0$ at the CNT free end to $s = L_{CNT}$ at the peeling point of attachment of the CNT to the AFM microcantilever. The parameter $\theta(s)$ describes local slope of the rod, and $z(s)$ describes the gap between the CNT and the substrate. The gap between the CNT and substrate at the peeling point is defined specifically as $\delta = z(L_{CNT})$, while P is the lateral force applied by the microcantilever at the peeling point.

The objective of the theoretical model is to predict P, the lateral force applied by the microcantilever at the peeling point, as a function of δ. In this model, δ is prescribed while P is calculated so that the interaction forces acting over the entire length of the CNT are balanced. The CNT−substrate interaction force per unit length varies along the CNT arc length depending on the CNT−substrate gap as shown by $f(z(s))$.

Following the work of Oyharcabal and Frisch,[27] the balance of moments and shear forces together with the elastica inextensibility leads to a system of three nondimensional ordinary differential equations

$$\frac{d^2\theta}{d\bar{s}^2}(\bar{s}) = -\bar{\gamma}(\bar{s})\cos\theta(\bar{s})$$

$$\frac{d\bar{\gamma}}{d\bar{s}}(\bar{s}) = \bar{f}(\bar{s})$$

$$\frac{dz}{d\bar{s}}(\bar{s}) = \sin\theta(\bar{s}) \qquad (1)$$

where $\bar{\gamma}(\bar{s})$ is the nondimensional shear force per unit length in the elastica and $\bar{f}(\bar{s})$ is the nondimensional CNT−substrate interaction force per unit length. These nondimensional quantities are related to the original (unbarred) dimensional s, $\gamma(s)$, $z(s)$, P, and $\delta(s)$ in the following manner

$$\bar{s} = \frac{s}{L_{CNT}}, \qquad \bar{\gamma}(\bar{s}) = \frac{L_{CNT}^2}{E_{CNT}I_{CNT}}\gamma(\bar{s})$$

$$\bar{z}(\bar{s}) = \frac{z(\bar{s})}{L_{CNT}}, \qquad \bar{f}(\bar{s}) = \frac{L_{CNT}^3}{E_{CNT}I_{CNT}}f(\bar{s})$$

$$\bar{\delta}(\bar{s}) = \frac{\delta(\bar{s})}{L_{CNT}}, \qquad \bar{P} = \frac{L_{CNT}^2}{E_{CNT}I_{CNT}}P \qquad (2)$$

As demonstrated by Coffin et al.,[7] the interaction between the outermost shell of the CNT and a graphitic surface can be derived from the universal graphitic potential of Girifalco et al.[25] For a multiwalled CNT (MWCNT), the contribution of the inner shells to the tube−substrate interaction forces is at least 1 order of magnitude smaller than of the outermost shell. Thus, while inner shell contributions play a significant role in the CNT stiffness, they can be neglected when modeling CNT−substrate interaction. Accordingly, the scaled interaction force per unit length $\bar{f}(\bar{s})$ is given by

$$\bar{f}(\bar{s}) = 6.119\alpha \left(\frac{L_{CNT}}{R_o - \rho}\right) \times \left(\left[\frac{1}{1 + \frac{0.09179 L_{CNT}}{R_o - \rho}\,\bar{z}(\bar{s})}\right]^5 - \left[\frac{1}{1 + \frac{0.09179 L_{CNT}}{R_o - \rho}\,\bar{z}(\bar{s})}\right]^{11}\right) \quad (3)$$

where α is a nondimensional quantity relating the strength of adhesive forces to the bending stiffness of the CNT and is given by

$$\alpha = \Phi_o \left(\frac{E_{CNT} I_{CNT}}{{L_{CNT}}^2}\right)^{-1} \quad (4)$$

such that Φ_o is the depth of the potential energy well per unit length between the CNT and substrate, which depends solely on the radius, R_o, of the outermost CNT shell.[25] The quantity ρ is the equilibrium separation between the graphite substrate and the center of the CNT, while L_{CNT}, E_{CNT}, and I_{CNT} are the respective length, elastic modulus, and cross-sectional area moment of the CNT. Notice in eq 3 that when the aspect ratio, represented by $(L_{CNT})/(R_o - \rho)$ is held constant, the nondimensionalized equations of eq 1 depend solely on the single nondimensional input parameter α, the ratio between the CNT−surface adhesion and CNT bending stiffness. For nanotubes of similar aspect ratios, α tends to be large for single-walled CNTs and small for multiwalled CNTs.

In accordance with experiment, the moment at the free end of the CNT must be zero, the slope of the peeling point must match the slope of the microcantilever (θ_o) depending on the specific AFM, and the shear force at the peeling point must balance the CNT−substrate interaction forces. Respectively, these boundary conditions are given by

$$\frac{d\theta}{d\bar{s}}(0) = 0, \qquad \theta(L_{CNT}) = \theta_o, \qquad \int_0^1 \bar{f}(\bar{s})\, d\bar{s} = \bar{P} \quad (5)$$

The ordinary differential equations of eq 1 with corresponding boundary conditions eq 5 were solved simultaneously in AUTO,[31] a software capable of numerically solving continuation and bifurcation problems in ordinary differential equations, to predict $\bar{P}$ as a function of $\bar{\delta}$.

Because of the interplay between adhesion and flexure, the model gives rise to some unique results, namely the coexistence of multiple stable configurations. The $\bar{P}$ versus $\bar{\delta}$ results are plotted in Figure 1b for an initially straight multiwalled CNT peeled from a highly order pyrolitic graphite (HOPG) substrate using parameter values that are typical for the CNT peeling probes. Figure 1b shows that for a given $\bar{\delta}$, multiple stable CNT equilibrium solutions exist where the CNT can either take s-shape, arc-shape, or freestanding configurations depending on the external loading $\bar{P}$. Each geometric configuration minimizes the total energy (U_T) of the system

$$U_T = \frac{E_{CNT} I_{CNT}}{2} \int_0^1 \left(\frac{d\theta}{d\bar{s}}\right)^2 d\bar{s} + \int_0^1 \bar{V}(\bar{z}(\bar{s}))\, d\bar{s} \quad (6)$$

where the first integral is the stored elastic energy (E_f) and the second integral is the sum of the interfacial energy (E_s), where $\bar{V} = \int \bar{f}(\bar{s})\, d\bar{z}$.

As $\bar{\delta}$ increases, the model predicts sudden transitions between different CNT configurations accompanied by sharp decreases in the magnitude of the applied force. In a s-shaped configuration, the CNT adheres to the substrate over most of its length and is detached from the substrate over a length scale comparable to the persistence length of the CNT. The s-shape configuration is the one that is typically studied using linear fracture mechanics.[32−34] The s-shaped configurations are characterized by both large interfacial and elastic strain energies. In an arc-shaped configuration, only the tip of the CNT adheres to the substrate. Arc-shaped configurations have negligible interfacial energies and high elastic strain energies. Our computational results suggest that the general shape of the $\bar{P}-\bar{\delta}$ curve, and the transitions between the s-shape, arc-shape, and freestanding configurations, also occur for single-walled CNTs and are fairly generic for one-dimensional nanostructures.

The above results do not take into account the mechanics of the force sensor, the AFM microcantilever, to which the CNT is attached. To account for this, we first note that the CNT applies both a bending moment and transverse shear force at the microcantilever free end. However, it can be shown that the contribution of the moment transfer is negligible. Accordingly, as shown in Figure 1a the microcantilever can simply be regarded as a linear spring of known stiffness, k_{cant}, that is attached to the CNT peeling end. In the AFM experiment, δ is not directly controlled. Instead, the microcantilever position z_r is gradually increased. When this occurs, Δ adjusts such that the elastic force of the microcantilever and the peeling force P equilibrate in which case $P = k_{cant}\Delta$. As a result, only specific parts of the $P-\delta$ curve will be accessible in an AFM experiment, as shown by the solid green line in Figure 1b. Thus, initially straight CNTs are expected to transition during peeling from s-shaped to arc-shaped to free-standing configurations, accompanied by sudden decreases in interfacial energy.

The theory was tested with dozens of multiwalled CNTs that were attached to the ends of tipless microcantilevers as shown in Figure 2 using a technique developed by Stevens et al.[35] The capability of reliably attaching the one-dimensional nanomaterial to the cantilever is critical to the success of the proposed method. While the attachment

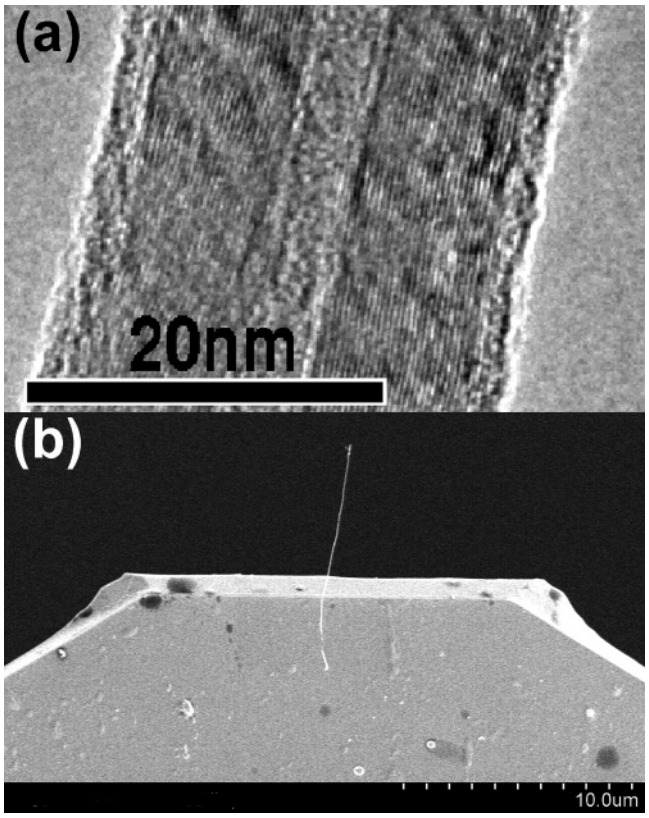

Figure 2. (a) Statistical analysis of the CNT source using transmission electron microscopy reveals the CNTs used for the peeling probes have inner and outer diameters of $d_i = 10 \pm 2$ nm and $d_o = 40 \pm 6$ nm. Tube lengths vary from 0.5 to 8 μm. (b) Scanning electron micrograph (SEM) of typical AFM peeling probes created by attaching a straight multiwalled CNT to the bottom of a tipless microcantilever.

procedure depends on the one-dimensional nanomaterial tested, numerous studies have shown the ability to directly manipulate and attach carbon fibers,[36] proteins,[18] and biological polymers[37] to the end of conical AFM tips. These processes could certainly be extended to the tipless cantilever used in the peeling experiment, where the surface area is larger and the positioning is less critical. When properly aligned, the CNTs naturally adhered to the microcantilever due to the van der Waals forces while an applied bias voltage (usually 5−15 V) would cause localized Joule heating at the CNT−microcantilever interface that welded the CNT to the microcantilever and eventually severed the CNT from the tungsten wire. The deviations from straightness of the CNTs tested were found to range from 1 to 20%. However, all results presented in this work are from CNTs with only 1% deviation from straightness.[38]

The nanomechanics of CNT peeling was studied using an Agilent 5500AFM system at room temperature in a chamber backfilled with dry nitrogen to minimize the influence of humidity. Static force−distance curves were acquired on freshly cleaved HOPG from SPI Supplies and on a silicon wafer with a thin layer of spin-coated 950PMMA from Microchem Corp.[39] Microcantilevers with stiffnesses in the range of 1−15 N/m were carefully chosen so that the signature CNT peeling event was discernible from the microcantilever pull-off. In general, microcantilevers with low stiffness should be used as they provide the best signal-to-noise ratio. However, if the microcantilever stiffness is too low, the microcantilever pull-off distance masks the peeling signature of the one-dimensional nanostructure. Future peeling probe designs should simultaneously reduce both stiffness and contact area.

The experimental results presented here concentrate on a few representative sets of results using CNTs with an initial 1% deviation from straightness, although the observed phenomena were also repeatable in CNTs with larger deviation from straightness. Most results were quantitatively repeatable under the same operating conditions at a given location on the sample. For a single peeling probe, results at different sample locations at different times are qualitatively repeatable. The static peeling spectroscopies of different peeling probes offer qualitatively similar results. While all of the experiments presented here were performed as pulling velocities between 1 and 5 μm/s near the upper limit of the AFM, slower speeds were also tested and did not have an effect on the results. The peeling speed may have an effect of the peeling signature of viscoelastic nanofibers, but it is unlikely to play a role in the largely elastic response of the MWCNTs tested.

When such a peeling probe approaches and retracts from a substrate, the peeling signature is evident in the force curve (see Figure 3). For instance a bare tipless probe exhibits the normal snap-in with large adhesive pull-off forces (Figure 3a). In comparison, for a peeling probe during retraction (Figure 3b), first the microcantilever pulls off after which the peeling signature of the one-dimensional nanostructure can be studied with nanoNewton (nN) force and nanometer (nm) distance resolution leading to an overall attoJoule (aJ) resolution of peeling or interfacial energies.

Figure 4 shows the full peeling force spectoroscopy curve for a straight CNT starting far from the surface (see part **I**) where neither the microcantilever nor the CNT interact with the approaching surface, and the force remains zero. Eventually, the probe snaps into the substrate due to van der Waals forces near $z_r = 0$. As z_r is decreased further, the microcantilever is bent upward leading to the positive repulsive forces recorded by part **II** of the curve. During retraction at $z_r \approx 10$ nm, the microcantilever pulls off the surface with an adhesion force of −60 nN, and the force returns to a value near zero. As z_r is increased further, the CNT peeling signature is recorded. The force magnitudes increase along part **III** of the curve to a value of −13 nN. At 200 nm, the magnitude of the force suddenly falls to zero. Further retraction leads to another increase of peeling force along the part of the curve labeled **IV**. Just beyond $z_r = 1800$ nm where the force reaches −16 nN, the peeling force jumps to zero. Upon still further retraction, the peeling force remains at zero, indicating the CNT has been fully released from the surface.

The experimental results of Figure 4 exhibit the same sudden force transitions predicted by the theoretical model: namely the CNT transition from s-shape to arc-shape configuration and later from an arc-shape to a freestanding

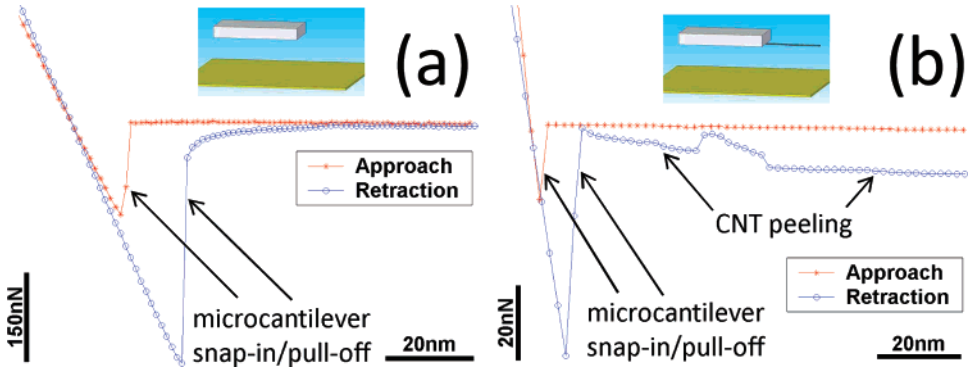

Figure 3. (a) Experimental forces curves using a bare, tipless cantilever on graphite demonstrating large pull-off forces. (b) Experimental force curves on a straight multiwalled CNT peeling probe with ≈1.5 μm length CNT that exhibit a classic peeling signature following the pull-off of the microcantilever. All force spectroscopy data discussed in this article are acquired from this peeling signature.

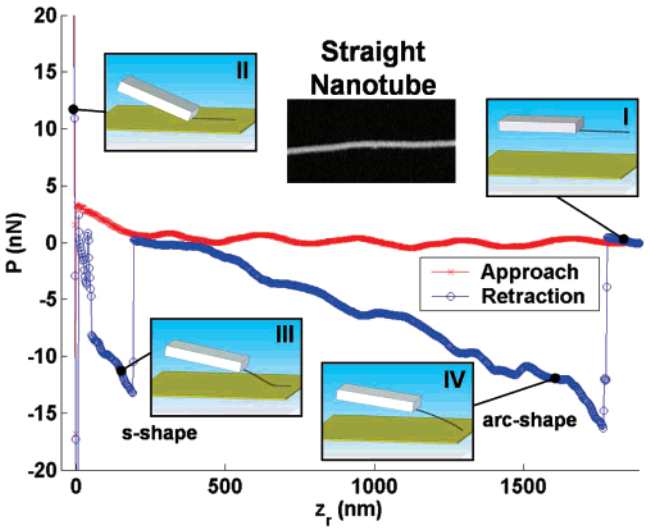

Figure 4. The full peeling force spectroscopy curve for a ≈1.5 μm length CNT typically shows two distinct regions of s-shaped and arc-shape states (graphic insets **III** and **IV**) and discontinuous transitions between them until the CNT is released into a freestanding state. The area of hysteresis is the total peeling energy and is specific to the nanotube-material surface tested. The curve has already been corrected for *z*-piezo nonlinearities by subtracting the *z*-piezo hysteresis measured far from the surface from the raw peeling data. Periodic ripples are due to laser interference from light reflecting off of the HOPG surface and do not correspond to actual applied forces.[47]

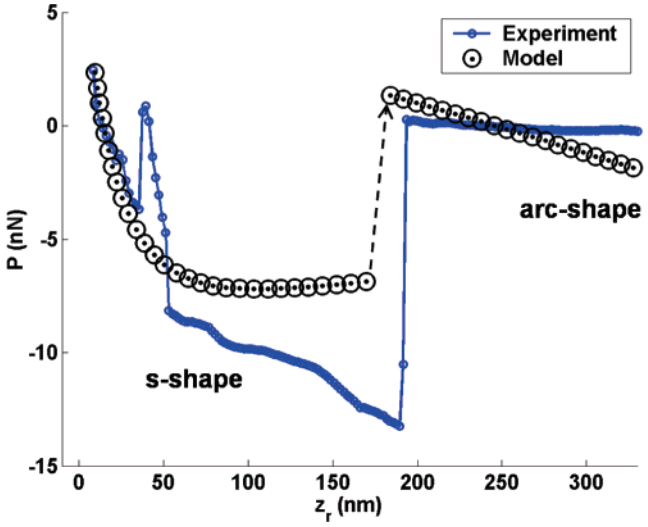

Figure 5. To match the theoretical predictions to the experimentally obtained results, the parameter α needs to be carefully selected (see eq 4). The CNT length (L_{CNT} ≈ 1.5 μm) was measured from its SEM image while d_o = 10 nm and d_i = 41 nm were assumed from the statistical averages of the CNT source. The potential energy well depth Φ_o = 14 nN is a function of the outer diameter.[25] Thus, E_{CNT} was adjusted to match the computational s-shape to arc-shape transition with experiment such that α = 0.13. The chosen modulus of E_{CNT} = 175 MPa agrees well with other CNTs grown via chemical vapor deposition.[48] The theory tends to underpredict slightly the adhesive forces in the s-shaped configurations but reasonably captures the overall shape of the force curve in the s-shaped region. On the other hand, the slope of the force distance curve in the arc-shaped region is not as well predicted.

configuration. To match theoretical predictions to experimental results for a CNT of given length, only the parameter α needs to be chosen to ensure a good fit. For example, when an appropriate value of α is chosen for the ≈1.5 μm CNT probe of Figure 4, we find that the theoretical predictions match reasonably well with the force curve in the s-shaped region as shown in Figure 5. In particular, the z_r range of existence of this configuration is well predicted theoretically while the theory tends to underestimate the value of the adhesive forces in this regime. This comparison between theory and experiment is typical for all the CNT peeling probes tested that exhibited a clear transition from the s-shaped to the arc-shaped configuration. A better match between theory and experiment would need to consider realistic effects such as the presence of a thin layer of amorphous carbon on the CNT, defects and slight initial curvature of the CNT, and presence of trapped charges on the HOPG surface. Because the model assumes vertical shear forces at the CNT−microcantilever interface, additional lateral forces such as those due to CNT−substrate friction are unaccounted in the model. The prediction of the force curve in the arc-shaped configuration is generally more error prone because the model includes only CNT wall interactions with the surface, not the CNT tip interactions.

It is interesting to consider the results of this work in the light of classical linear fracture mechanics that is used to measure interfacial energies for microscale systems.[32] According to this theory, the gap between the cantilevered CNT

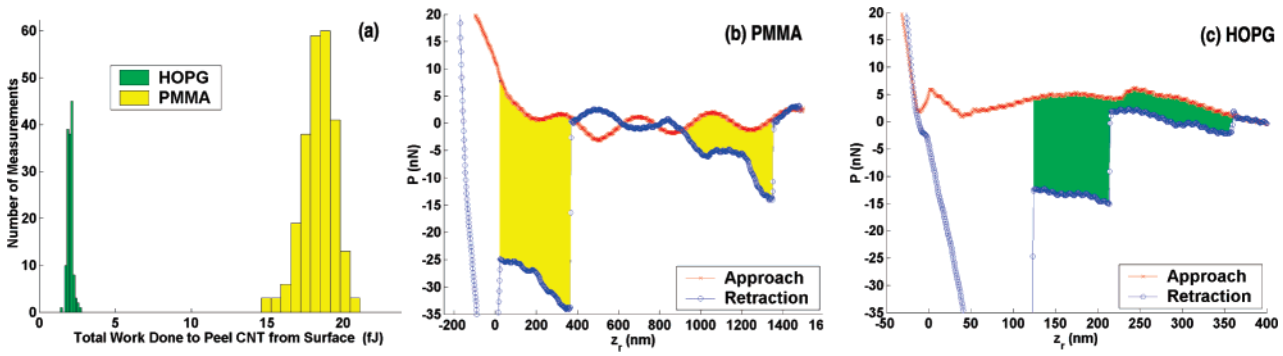

Figure 6. (a) The total peel energy extracted and plotted from hundreds of static peeling experiments performed using with panel a ≈1.8 μm length CNT probe on HOPG and the polymer PMMA. The peeling energy for the same nanotube on a PMMA surface is an order of magnitude greater than on HOPG. A typical static peeling spectroscopy for (b) PMMA shows a large hysteresis between approach and retraction particularly in the s-shaped configuration compared to the (c) static peeling curve on HOPG. Thus, more energy is needed to peel the CNT from PMMA because of its larger surface energy.

and the substrate in the s-shaped configuration can be regarded as a nanoscale crack, which is gradually opened in a mode I fracture during the AFM peeling experiment. For a quasi-static situation, the crack length equilibrates to allow the energy release rate per unit length G to equal Γ, the interfacial adhesion energy per unit length. For a cantilevered CNT adhered to a surface

$$G = 18\frac{E_{CNT}I_{CNT}\delta^2}{\lambda^4} \tag{7}$$

where E_{CNT} and I_{CNT} are, respectively, the elastic modulus and area moment of the CNT, δ is the crack tip opening at the peeling point of the CNT, and λ is total crack length of the portion of the CNT released from the surface. Thus, calculation of the interfacial surface energy requires a knowledge of the crack length. However, for one-dimensional nanostructures, this recourse is not presently available and so explicit measurements of the interfacial surface energy are still beyond reach. For this, peeling force spectroscopy needs to be performed with in situ, high-resolution electron microscopy to observe the shape of the deforming nanostructure. Such a capability will greatly benefit the development of a standardized nanomechanical peel test.

The peeling force spectrograms can be used to measure the work needed to completely peel a CNT off the substrate, which in turn can be used to quickly compare interaction energies of CNTs and different samples directly. During a signature peeling event like that shown by the retraction curve in Figure 4, the microcantilever does work on the adhered CNT as it applies a measured force through a known distance. The total peel work is found from the area of hysteresis between the approach and retraction curves from the point that the AFM microcantilever is released until the CNT reaches its freestanding state. Because the area of hysteresis for the straight CNT in Figure 4 includes CNT transitions from s-shape to arc-shape configurations, the total work needed to peel the CNT includes both the energy needed to overcome adhesion and energy temporarily stored in CNT deformations.

To demonstrate this, a single CNT peeling probe has been used to perform hundreds of peeling force spectroscopy experiments on HOPG and then on polymethyl-methacrylate (PMMA) under the same set of conditions. The total peeling energy required to remove the CNT was calculated for each test, and the results are presented in Figure 6. As expected, the peel energy required to remove a CNT from the PMMA polymer sample was much larger than HOPG. When one compares the adhesion forces in the s-shaped configurations on both surfaces, it is clear that the adhesion between the CNT and PMMA is much stronger than CNT and HOPG, as more work is required to separate the two surfaces. Thus, the AFM peeling spectroscopy is a sensitive tool to quantitatively compare the CNT−substrate interaction energies between different substrate materials.

We have developed a theoretical model and adapted the AFM to investigate the nonlinear nanomechanics of peeling one-dimensional nanostructures from different material substrates. Theory and experimental force curves clearly indicate that multiwalled CNTs undergo sudden configurational changes with sequentially decreasing interfacial energies. The coexistence of and transition between different configurations (s-shaped, arc-shaped, or freestanding) of straight one-dimensional nanostructures has important implications for the control of adhesion and stiction in nanoelectromechanical systems, artificial gecko setae, CNT-based flash memories and switches, and for the effective dispersion of CNTs and nanofibers in the manufacture of nanocomposites. For instance, intentional external perturbations in the form of ultrasound[33,40] or electrostatic forces[41] could trigger the transition of an adhering nanotube or nanowire from an s-shaped configuration to an arc-shaped or freestanding configuration to greatly reduce adhesion in an active, controlled manner. In contrast to the few available techniques[42,43] that are capable of measuring interaction energies between nanoscale fibers and matrix materials, the new peeling spectroscopy technique offers the ability to sensitively compare adhesion characteristics with minimal preparation. The ability to efficiently compare adhesion between CNTs and different polymers opens the door to screening of different fiber coatings/functionalizations.[44,45] Ultimately, an improved understanding of the nanomechanics of stiction and the development of a standardized nanomechanical peel test could broadly benefit the development of nanoelectronic

devices, biomedical devices and materials, biomimetic adhesives, and nanocomposite materials.

Acknowledgment. A.R. gratefully acknowledges financial support for this research provided by the National Science Foundation (CMMI 0700289) and the Korean Center for Nanomanufacturing and Mechatronics (Dr. C. S. Han). C.V.N is employed by ELORET Corporation at NASA Ames Research Center, and his work is supported by a subcontract from University Affiliated Research Center (UARC) operated by the University of California Santa Cruz at NASA Ames.

References

(1) Cook, J. W.; Edge, S.; Packham, D. E. *Int. J. Adhes. Adhes.* **1997**, *17*, 333−337.
(2) Bagchi, A.; Evans, A. G. *Interface Sci.* **1996**, *3*, 169−193.
(3) Correa-Duarte, M. A.; Wagner, N.; Rojas-Chapana, J.; Morsczek, C.; Thie, M.; Giersig, M. *Nano Lett.* **2004**, *4*, 2233−2236.
(4) Sever, M. J.; Weisser, J. T.; Monahan, J.; Srinivasan, S.; Wilker, J. J. *Angew. Chem., Int. Ed.* **2004**, *43*, 448−450.
(5) Correa-Duarte, M. A.; Wagner, N.; Rojas-Chapana, J.; Morsczek, C.; Thie, M.; Giersig, M. *Nano Lett.* **2004**, *4*, 2233−2236.
(6) Shi, X.; Kong, Y.; Zhao, Y.; Gao, H. *Acta Mech. Sin.* **2005**, *21*, 249−256.
(7) Coffin, D. W.; Carlsson, L. A.; Pipes, R. B. *Compos. Sci. Technol.* **2006**, *66*, 1132−1140.
(8) Strus, M. C.; Raman, A.; Han, C.-S.; Nguyen, C. V. *Nanotechnology* **2005**, *16*, 2482−2492.
(9) Jang, J. E.; Cha, S. N.; Choi, Y.; Amaratunga, G. A. J.; Kang, D. J.; Hasko, D. G.; Jung, J. E.; Kim, J. M. *Appl. Phys. Let.* **2005**, *87*, 163114.
(10) Dujardin, E.; Derycke, V.; Goffman, M. F.; Lefèvre, R.; Bourgoin, J. P. *Appl. Phys. Let.* **2005**, *87*, 193107.
(11) Mahar, B.; Laslau, C.; Yip, R.; Sun, Y. *IEEE Sens. J.* **2007**, *7*, 266−284.
(12) Baibarac, M.; Gomez-Romero, P. *J. Nanosci. Nanotechnol.* **2006**, *6*, 289−302.
(13) Desai, A. V.; Haque, M. A. *Thin Wall. Struct.* **2005**, *43*, 1787−1803.
(14) White, A. A.; Best, A. M.; Kinloch, I. A. *Int. J. Appl. Ceram. Technol.* **2007**, *297*, 1−13.
(15) Breuer, O.; Sungararaj, U. *Polym. Compos.* **2004**, *25*, 630−645.
(16) Domke, J.; Radmacher, M. *Langmuir* **1998**, *14*, 3320−3325.
(17) Rotsch, C.; Braet, F.; Eisse, E.; Radmacher, M. *Cell Biol. J.* **1997**, *21*, 685−696.
(18) Zlatanova, J.; Lindsay, S. M.; Leuba, S. H. *Prog. Biophys. Mol. Biol.* **2000**, *74*, 37−61.
(19) Marszalek, P. E.; Li, H.; Oberhauser, A. F.; Fernandez, J. M. *Proc. Natl. Acad. Sci. U.S.A.* **2002**, *99*, 4278−4823.
(20) Kendall, K. *J. Phys. D: Appl. Phys.* **1975**, *8*, 1449−1452.
(21) Aksak, B.; Murphy, M. P.; Sitti, M. *Langmuir* **2007**, *23*, 3322−3332.
(22) Li, Q.; Koo, S.-.; Richter, C. A.; Edelstein, M. D.; Bonevich, J. E.; Kopanski, J. J.; annd E. M Vogel, J. S. S. *IEEE Trans. Nanotechnol.* **2007**, *6*, 256−262.
(23) Xie, X.-L.; Mai, Y.-W.; Zhou, X.-P. *Mater. Sci. Eng., R* **2005**, *49*, 89−112.
(24) Love, A. E. H. *A Treatise on the Mathematical Theory of Elasticity*; Dover Publications: New York, 1944.
(25) Girifalco, L. A.; Hodak, M.; Lee, R. S. *Phys. Rev. B* **2005**, *62*, 103104−13110.
(26) Delrio, F. W.; Boer, M. P. D.; Knapp, J. A.; E. D. R., Jr.; Clews, P. J.; Dunn, M. L.; Reedy, E. D., Jr. *Nature* **2005**, *5*, 629−634.
(27) Oyharcabal, X. F. T. *Phys. Rev. E* **1999**, *71*, 036611.
(28) Majidi, C. S.; Groff, R. E.; Fearing, R. S. *J. Appl. Phys.* **2005**, *98*, 103521.
(29) Purohit, P. K.; Kondev, J.; Phillips, R. *Proc. Natl. Acad. Sci. U.S.A.* **2003**, *100*, 3173−3178.
(30) Treacy, M. M. J.; Ebbesen, T. W.; Gibson, J. M. *Proc. Natl. Acad. Sci. U.S.A.* **1996**, *381*, 678−680.
(31) Doedel, E. J.; Keller, H. B.; Kernévez, J. P. *Int. J. Bifurcation Chaos Appl. Sci. Eng.* **1991**, *1*, 493−520.
(32) Treacy, M. M. J.; Ebbesen, T. W.; Gibson, J. M. *J. Appl. Phys.* **1999**, *86*, 817−827.
(33) Savkar, A. A.; Murphy, K. D.; Leseman, Z. C.; Mackin, T. J.; Begley, M. R. *J. Microelectromech. Syst.* **2007**, *16*, 163−173.
(34) Rogers, J. W.; Mackin, T. J.; Phinney, L. M. *J. Microelectromech. Syst.* **2002**, *11*, 512−520.
(35) Stevens, R.; Nguyen, C. V.; Cassell, A.; Delzeit, L.; M, M. M.; Han, J. *Appl. Phys. Lett.* **2000**, *77*, 3453−3455.
(36) Jung, S. I.; Choi, J. S.; Shim, H. C.; Kim, S.; Jo, S. H.; Lee, C. J. *Appl. Phys. Lett.* **2006**, *89*, 233108.
(37) Gu, J.; Xiao, Z.; Yam, C.-M.; Qin, G.; Deulge, M.; Boutet, S.; Cai, C. *Biophys. J.* **2005**, *89*, L31−L33.
(38) Deviation from straightness κ for a CNT was calculated from the side SEM image of a CNT. The CNT image was curve-fitted with a straight line, and the deviation from that line, ζ_n, was calculated for each point along the CNT. Then $\kappa = \sqrt{\Sigma\zeta_n^2}/L_{\mathrm{CNT}}$.
(39) The experimental procedure began by first minimizing the angular tilt of the sample relative to the microcantilever by monitoring and minimizing the torsion signal. The microcantilever stiffness was calibrated by first finding the quality factor, or Q-factor, from the unconstrained frequency sweep and applying the method developed by Sader et al,[46] while the microcantilever sensitivity was obtained from the static deflection curve where the microcantilever with attached CNT is pressed into the hard HOPG sample. According to AFM topography scans, HOPG surfaces were almost atomically flat while the PMMA sample had an surface roughness less than 3 nm per 2.5 μm^2.
(40) Socoliuc, A.; Gnecco, E.; Maier, S.; Pfeiffer, O.; Baratoff, A.; Bennewitz, R.; Meyer, E. *Science* **2007**, *313*, 207−209.
(41) Knapp, J. A.; de Boer, M. P. *J. Microelectromech. Syst.* **2002**, *11*, 754−764.
(42) Barber, A. H.; Cohen, S. R.; Wagner, H. D. *Appl. Phys. Let.* **2003**, *82*, 4140−4142.
(43) Nuriel, S.; Katz, A.; Wagner, H. D. *Composites, Part A* **2005**, *36*, 33−37.
(44) Star, A.; Stoddart, J. F.; Steuerman, D.; Diehl, M.; Boukai, A.; Wong, E. W.; Yang, X.; Chung, S.-W.; Choi, H.; Heath, J. R. *Angew. Chem., Int. Ed.* **2001**, *40*, 1721−1725.
(45) Lin, Y.; Meziani, M. J.; Sun, Y.-P. *J. Mater. Chem.* **2007**, *17*, 1143−1148.
(46) Sader, J. E.; Chon, J. W. M. *Rev. Sci. Instrum.* **1999**, *70*, 3967−3969.
(47) Jaschke, M.; Butt, H.-J. *Rev. Sci. Instrum.* **1995**, *66*, 1258−1259.
(48) Gaillard, J.; Skove, M.; Rao, A. M. *Appl. Phys. Let.* **2006**, *86*, 233109.

NL0728118